

Dark Matter Searches: The Nightmare Scenario

Gianfranco Bertone^{1,2}, Daniel Cumberbatch³, Roberto Ruiz de Austri⁴ and Roberto Trotta^{5,6}

¹*Institute for Theoretical Physics, Univ. of Zürich, Winterthurerst. 190, 8057 Zürich, CH*

²*Institut d'Astrophysique de Paris, UMR 7095-CNRS, Univ. P. et M. Curie, 98bis Bd Arago, 75014 Paris, France*

³*Astroparticle Theory and Cosmology Group, University of Sheffield, Hicks Building, Hounsfield Road, Sheffield, South Yorkshire, S3 7RH, UK*

⁴*Instituto de Física Corpuscular, IFIC-UV/CSIC, Apartado 22085, E-46071 Valencia, Spain*

⁵*Astrophysics Group, Imperial College London, Blackett Laboratory, Prince Consort Road, London SW7 2AZ, UK*

⁶*Kavli Institute for Theoretical Physics, Kohn Hall, University of California, Santa Barbara, CA 93106-4030, USA*

Email: bertone@iap.fr, d.cumberbatch@sheffield.ac.uk, rruiz@ific.uv.es, r.trotta@imperial.ac.uk

ABSTRACT: The unfortunate case where the Large Hadron Collider (LHC) fails to discover physics Beyond the Standard Model (BSM) is sometimes referred to as the “Nightmare scenario” of particle physics. We study the consequences of this hypothetical scenario for Dark Matter (DM), in the framework of the constrained Minimal Supersymmetric Standard Model (cMSSM). We evaluate the surviving regions of the cMSSM parameter space after null searches at the LHC, using several different LHC configurations, and study the consequences for DM searches with ton-scale direct detectors and the IceCube neutrino telescope. We demonstrate that ton-scale direct detection experiments will be able to conclusively probe the cMSSM parameter space that would survive null searches at the LHC with 100 fb^{-1} of integrated luminosity at 14 TeV. We also demonstrate that IceCube (80 strings plus DeepCore) will be able to probe as much as $\simeq 17\%$ of the currently favoured parameter space after 5 years of observation.

Contents

1. Introduction	1
2. Theoretical Setup	3
2.1 The cMSSM	3
2.2 Statistical framework	3
2.3 Priors	4
2.4 Cosmological and collider constraints	6
2.5 LHC constraints	6
3. Results	7
3.1 The cMSSM after null searches at the LHC	7
3.2 Implications for Direct detection	8
3.3 Implications for indirect detection with the IceCube neutrino telescope	12
3.4 The role of the Higgs	17
4. Discussion and Conclusions	18

1. Introduction

One of the main goals of the Large Hadron Collider (LHC) at CERN is to test the existence of physics Beyond the Standard Model (BSM), especially in view of the possible connection with the problem of Dark Matter (DM) in astrophysics and cosmology [1]. Recently, the ATLAS and CMS experimental collaborations have published the results of the first LHC searches for Supersymmetry (SUSY) [2, 3, 4, 5, 6, 7], based on $\sqrt{s} = 7$ TeV collisions recorded during 2010. The absence of any excess above Standard Model (SM) predictions allows one to already set interesting constraints on BSM physics, and several groups of authors have already studied the impact of these results on Supersymmetric scenarios (see, e.g., [8, 9, 10, 11, 12, 13, 14]).

The prospects for discovering BSM physics at the LHC and the consequences for Dark Matter searches have been thoroughly discussed in the literature. In particular, we have recently discussed the case of positive detection both at the LHC *and* with Dark Matter

experiments [15]. Here, we focus instead on the unfortunate case where the LHC *fails* to discover BSM physics, a scenario sometimes referred to as the “Nightmare scenario” of particle physics (see, e.g., [16] and references therein). We focus on the constrained Minimal Supersymmetric Standard Model (cMSSM) [17, 18, 19, 20, 21], for which detailed studies exist regarding the reach of the LHC for various configurations of beam energy and total integrated luminosity.

The main focus of this paper is to analyse the consequences of the nightmare scenario for Dark Matter searches. These can be actually divided into two broad classes, viz. *direct* and *indirect* searches (for recent reviews see, e.g., [1, 22, 23, 24, 25]). Direct searches are based on the search for rare nuclear recoils due to the scattering of Dark Matter particles off nuclei in underground experiments. There are many undergoing and upcoming experiments (see, e.g., [26] for a discussion of upcoming experimental capabilities), and despite some intriguing signals that have been discovered by the DAMA/LIBRA [27] and, more recently, the CoGeNT [28, 29, 30] collaborations, it appears difficult to reconcile a standard Dark Matter interpretation of these results with other experimental findings, in particular with the null searches from XENON-100 [31] or CDMS II [32] (see, e.g., the discussions in [33, 34, 35, 36]).

Indirect searches are based instead on the astrophysical searches for secondary particles produced in the annihilation or decay of Dark Matter particles. Despite the huge interest attracted by astrophysical data (see, in particular, the plethora of literature devoted to explaining the positron excess recently measured by PAMELA [37]), a convincing identification of Dark Matter based on these data seems problematic, due to the lack of strong constraints on the properties of Dark Matter particles as well as to the poor control of astrophysical backgrounds and associated systematics (see, e.g., the discussion in [16]). Among the possible smoking-gun signals that can be obtained with indirect searches, we will focus on one of the most intriguing, and less affected by astrophysical uncertainties: the detection of high-energy neutrinos from the centre of the Sun [38] using the IceCube neutrino telescope, which is located at the geographical South Pole (see, e.g., [39]).

We show here that upcoming ton-scale direct detection (DD) experiments, and to a lesser extent IceCube, can actually probe a large portion of cMSSM parameter space that will remain unconstrained in the nightmare scenario, and therefore represent *a unique opportunity to discover new physics by the end of the decade*, in case of null searches at the LHC.

The paper is organized as follows: in Sec. 2 we introduce our theoretical framework, i.e., the cMSSM, and we present the statistical tools adopted to identify the region of cMSSM parameter space corresponding to the LHC *nightmare* scenario; in Sec. 3 we present our results and discuss the consequences for Dark Matter searches; and, finally, in Sec. 4 we provide a brief summary.

2. Theoretical Setup

2.1 The cMSSM

Supersymmetry (SUSY) is one the most compelling extensions of the Standard Model of Particle Physics, and the Supersymmetric neutralino is among the best-motivated Dark Matter (DM) candidates (for a review of SUSY DM candidates see, e.g., [40, 24, 25].)

Neutralinos are the mass eigenstate of a mixture of bino, wino (superpartners of the B and W^0 gauge bosons respectively) and two higgsinos (superpartners of the H_1^0, H_2^0 Higgs bosons). In many realizations of the Minimal Supersymmetric Standard Model (MSSM), the lightest among the four neutralinos is the lightest SUSY particle, which is made stable by virtue of the conservation of R-parity. It is commonly referred to as “the” neutralino, χ_1^0 , and constitutes a popular DM candidate, adopted by much of the relevant literature.

Since superpartners of Standard Model particles have not been observed, SUSY must be broken at some energy scale. Over the past few decades, several SUSY-breaking mechanisms have been proposed in the literature (for a recent review see, e.g., [41]). Perhaps the most appealing of these regards gravity as the means of communication between a hidden sector, where SUSY breaking occurs, and the visible sector [21]. In the so-called constrained Minimal Supersymmetric Standard Model (cMSSM) [17, 18, 19, 20, 21], which is the model focussed upon in this paper, the mechanism via which SUSY is broken nor how this breaking is transmitted to the visible sector need be specified, so long as the latter occurs at or near the GUT scale. In the cMSSM the soft parameters are assumed universal at a high scale (M_X), hence the parameter space of the model is defined in terms of four free parameters and one sign: the common scalar mass (m_0), the common gaugino mass ($m_{1/2}$) and the tri-linear mass (A_0) parameters (all specified at the GUT scale), plus the ratio of Higgs vacuum expectation values $\tan\beta$ and $\text{sign}(\mu)$, where μ is the higgsino mass parameter whose value is determined from the conditions of radiative electroweak symmetry breaking.

2.2 Statistical framework

We denote the parameter set of the cMSSM (i.e., $m_0, m_{1/2}, A_0$ and $\tan\beta$) by θ , where we fix $\text{sgn}(\mu)=+1$, motivated by consistency arguments involving measurements of the anomalous muon magnetic moment, which can only be explained with a positive μ [42] (see also, e.g., [43]), while ψ denotes the relevant SM quantities that enter into the calculation of observable quantities (the so-called “nuisance parameters”), namely

$$\psi \equiv \{M_t, m_b(m_b)^{\overline{MS}}, \alpha_s(M_Z)^{\overline{MS}}, \alpha_{\text{em}}(M_Z)^{\overline{MS}}\}, \quad (2.1)$$

where M_t is the pole top quark mass, $m_b(m_b)^{\overline{MS}}$ is the bottom quark mass at m_b , while $\alpha_{\text{em}}(M_Z)^{\overline{MS}}$ and $\alpha_s(M_Z)^{\overline{MS}}$ are the electromagnetic and the strong coupling constants at the Z pole mass M_Z , the last three being evaluated in the \overline{MS} scheme. We denote the full 8-dimensional parameter set by

$$\Theta = (\theta, \psi). \quad (2.2)$$

The cornerstone of Bayesian inference is Bayes’ Theorem, which reads

$$p(\Theta|d) = \frac{p(d|\Theta)p(\Theta)}{p(d)}. \quad (2.3)$$

The quantity $p(\Theta|d)$ on the l.h.s. of Eq. (2.3) is known as the *posterior*, while on the r.h.s., the quantity $p(d|\Theta)$ is the *likelihood* (when taken as a function Θ for fixed data, d). The quantity $p(\Theta)$ is the *prior* which encodes our state of knowledge about the values of the parameters Θ before scrutinising the data. Our state of knowledge is then updated to the posterior via the likelihood. Finally, the quantity in the denominator of Eq. (2.2) is known as the *evidence* or *model likelihood*. If one is interested in constraining the model’s parameters, the evidence is merely a normalization constant, independent of Θ , and can therefore be dropped by converting Eq. (2.3) into a proportionality relation (see, e.g., [44] for further details).

In order to explore the posterior of Eq. (2.3) in an efficient way, we adopt the **MultiNest** [45] algorithm, as implemented in the public package **SuperBayeS-v1.5**. **MultiNest** provides an extremely efficient sampler even for likelihood functions defined over a parameter space of large dimensionality with a very complex structure. This aspect is very important for exploring the cMSSM, as previous MCMC scans have revealed that the 8-dimensional likelihood surface is very fragmented and that it presents many finely-tuned regions that are difficult to explore with conventional MCMC scans (and almost impossible to find with conventional grid scans) (see also, e.g., [46, 47] for further discussions of these aspects).

2.3 Priors

In order to perform our scan over the cMSSM and SM nuisance parameters, we need to specify our prior in Eq. (2.3). The role of the prior is to define a statistical measure on the parameter space. In principle, when the likelihood is strongly constraining (i.e., for accurate data) the posterior is dominated by the likelihood and the choice of prior is irrelevant, as the information in the likelihood completely overrides the information in the prior. However, it has been shown that this is presently not the case for the cMSSM, i.e., different, plausible, choices of priors lead to different posteriors and hence different inferences on cMSSM parameter space [48], although inclusion of recent direct detection constraints from XENON-100 does mitigate the problem [14]. It is expected that a complete resolution of this issue will come from future, more detailed, data and, in particular, measurements of the SUSY mass spectrum by the LHC, which will conclusively resolve ambiguities brought about by prior dependences in case SUSY is discovered [49].

In this paper, we adopt two sets of widely used priors, namely the so-called “flat priors” (uniform on the scalar and gaugino masses) and the “log-priors” (uniform on the log of the masses). Both sets of priors are uniform in A_0 and $\tan\beta$. By considering two choices of priors, we can assess the residual prior dependency of our conclusions. The prior ranges

Observable	Mean value	Uncertainties		ref.
	μ	σ (exper.)	τ (theor.)	
M_W [GeV]	80.398	0.025	0.015	[50]
$\sin^2 \theta_{eff}$	0.23153	0.00016	0.00015	[50]
$\delta a_\mu^{SUSY} \times 10^{10}$	29.6	8.1	2.0	[51]
$BR(\bar{B} \rightarrow X_s \gamma) \times 10^4$	3.55	0.26	0.30	[52]
ΔM_{B_s} [ps $^{-1}$]	17.77	0.12	2.40	[53]
$\frac{BR(B_u \rightarrow \tau \nu)}{BR(B_u \rightarrow \tau \nu)_{SM}}$	1.28	0.38	-	[52]
$\Delta_{0-} \times 10^2$	3.6	2.65	-	[54]
$\frac{BR(B \rightarrow D \tau \nu)}{BR(B \rightarrow D e \nu)} \times 10^2$	41.6	12.8	3.5	[55]
R_{l23}	1.004	0.007	-	[56]
$BR(D_s \rightarrow \tau \nu) \times 10^2$	5.38	0.32	0.2	[52]
$BR(D_s \rightarrow \mu \nu) \times 10^3$	5.81	0.43	0.2	[52]
$BR(D \rightarrow \mu \nu) \times 10^4$	3.82	0.33	0.2	[52]
$\Omega_\chi h^2$	0.1123	0.0035	10%	[57]
	Limit (95% CL)		τ (theor.)	ref.
$BR(\bar{B}_s \rightarrow \mu^+ \mu^-)$	$< 5.8 \times 10^{-8}$		14%	[58]
m_h	> 114.4 GeV		3 GeV	[59]
ζ_h^2	$f(m_h)$ as defined in [61]			[59]
$m_{\tilde{q}}$	> 375 GeV		5%	[60]
$m_{\tilde{g}}$	> 289 GeV		5%	[60]
other sparticle masses	As in Table 4 of [61].			[61]

Table 1: Experimental data used for the computation of the likelihood function. For each row, the central value is given, together with the experimental and theoretical uncertainty.

SM (nuisance) parameter	Mean value μ	Uncertainty σ (exp.)	Ref.
M_t	173.1 GeV	1.3 GeV	[62]
$m_b(m_b)^{\overline{MS}}$	4.20 GeV	0.07 GeV	[60]
$\alpha_s(M_Z)^{\overline{MS}}$	0.1176	2×10^{-3}	[60]
$1/\alpha_{em}(M_Z)^{\overline{MS}}$	127.955	0.03	[63]

Table 2: Experimental mean μ and standard deviation σ adopted for the likelihood function for SM (nuisance) parameters, assumed to be described by a Gaussian probability distribution function.

we use are given by

$$\begin{aligned}
50 \text{ GeV} &\leq m_0, m_{1/2} \leq 4000 \text{ GeV} \\
|A_0| &\leq 7 \text{ TeV} \\
2 &< \tan \beta < 62.
\end{aligned}$$

2.4 Cosmological and collider constraints

In order to derive current constraints on cMSSM parameters, we perform a global scan for both approaches using flat priors on the model parameters, including in the likelihood current cosmological and collider experimental constraints, as displayed in Table 1, and with constraints on the SM nuisance parameters as displayed in Table 2. In this paper, we utilise the same likelihood function as in [14], invoking the experimental constraints listed in Table 1. We refer the reader to [61] for a detailed description of the likelihood function. In particular, we include the measurement of the anomalous magnetic moment of the muon based on e^+e^- data, which gives a 3.7σ discrepancy with the SM predicted value [51].

We compute $\delta_{\text{had}}^{\text{SM}}a_\mu$ at full one-loop level adding the logarithmic piece of the quantum electro-dynamics two-loop calculation [64]. The $BR(\overline{B} \rightarrow X_s \gamma)$ branching ratio (which has been shown to provide an important constraint, see, e.g., the recent study [65]), has been computed with the numerical code **SusyBSG** [66] using the full NLO QCD contributions, including the two-loop calculation of the gluino contributions presented in [67] and the results of [68] for the remaining non-QCD $\tan\beta$ -enhanced contributions. For the determination of ΔM_{B_s} we use expressions from [69] which include dominant large $\tan\beta$ -enhanced beyond-LO SUSY contributions from Higgs penguin diagrams. The other B(D)-physics observables summarized in Table 1 have been computed with the code **SuperIso** (for details on the computation of the observables see, e.g., [70] and references therein). Both codes have been integrated into **SuperBayes**. We discard points that do not fulfill the conditions of radiative electroweak symmetry breaking and/or give non-physical (i.e., tachyonic) solutions.

We also include the constraints on the cold Dark Matter (CDM) relic abundance determined from the 7-year WMAP data [57] to constrain the relic abundance $\Omega_\chi h^2$ of the lightest neutralino, which we assume represents the sole constituent of CDM in the Universe, by invoking a conventional Gaussian pdf in the likelihood (with an additional 10% theoretical error).

The constraints imposed by the recent LHC data are described in detail in Sec. 2.5.

2.5 LHC constraints

The LHC at CERN started operations in September 2008, marking the beginning of an intensive period of investigation. The current plan (as of Summer 2011) is that the LHC will be running at the current centre of mass energy $\sqrt{s} = 7\text{ TeV}$ throughout 2012. Following this period, an approximately 18 month maintenance period is expected to commence in order to upgrade the LHC, after which the first attempts at collisions with $\sqrt{s} = 14\text{ TeV}$ are expected.

Whilst the discovery of SUSY would obviously be of paramount importance, the task of actually identifying weakly-interacting massive particles (WIMPs) as the dominant constituent of DM using LHC data alone is challenging [71], unless complementary information is provided by other experiments, e.g., by direct [15] or indirect [72] searches, or by specific

accelerator signatures, such as the shape of the dilepton invariant mass spectrum in the MSSM focus point region [73].

To compute the region of the cMSSM parameter space where the LHC will be able to achieve a 5σ discovery, we consider studies conducted by the ATLAS collaboration for a centre of mass energy of 14 TeV and an integrated luminosity (IL) of 1 fb^{-1} [74] (which is expected to be achieved by 2014–2015)¹. We have adopted the analysis consisting in looking for events containing 4 jets + 0 leptons + \cancel{E}_T which have been performed for fixed $A_0 = 0, \tan \beta = 10$ values. Nevertheless these sort of analyses are relatively insensitive to $\tan \beta$ and A_0 due to the fact that large $\tan \beta$ values, basically, alter the phenomenology of multilepton production channels [79] which are not considered here. We have followed the procedure described in [80] for implementing the $\sqrt{s} = 14 \text{ TeV}$ and $\text{IL} = 100 \text{ fb}^{-1}$ LHC configuration (representing what might be achieved over a timescale of about 10 years). In this case, the authors have optimized the search looking for events containing a number of jets $> 2 + n = 0, \dots, 6$ leptons + \cancel{E}_T where $A_0 = 0, \tan \beta = 45$ values have been assumed. Studies of this sort have shown that the detectability level exhibits only a mild dependence on A_0 and $\tan \beta$ [81]. Therefore, although the resulting LHC sensitivity is expressed as a detection region in the $m_0, m_{1/2}$ plane for fixed values of A_0 and $\tan \beta$, we assume it to be universal for all values of A_0 and $\tan \beta$, as argued above.

3. Results

3.1 The cMSSM after null searches at the LHC

We begin by displaying in Fig. 1 the favoured region of the cMSSM parameter space (in terms of the Bayesian posterior pdf) in the $(m_0, m_{1/2})$ plane, where we have marginalized over all other parameters. The top and bottom rows show results for the flat and log priors respectively. From left to right, we have imposed current LHC constraints (left panels), and future constraints assuming that the LHC does not detect SUSY with $\sqrt{s} = 14 \text{ TeV}$ and $\text{IL} = 1 \text{ fb}^{-1}$ (middle panels) and $\sqrt{s} = 14 \text{ TeV}$ and $\text{IL} = 100 \text{ fb}^{-1}$ (right panels). This has been achieved by removing samples which lie below the 5σ detection region, depicted by the magenta dot-dashed curve for the LHC with $\sqrt{s} = 14 \text{ TeV}$ and $\text{IL} = 1 \text{ fb}^{-1}$, and by the solid blue curve for $\sqrt{s} = 14 \text{ TeV}$ and $\text{IL} = 100 \text{ fb}^{-1}$.

With the current LHC configuration, both the stau co-annihilation and h -pole regions remain inaccessible. The latter (visible as a small, vertical sliver of probability at small values of $m_{1/2}$) we see will become accessible with an integrated luminosity of 1 fb^{-1} and a centre of mass energy of 14 TeV. For an LHC configuration of $\sqrt{s} = 14 \text{ TeV}$ and $\text{IL} = 100 \text{ fb}^{-1}$, we see that the stau co-annihilation region displayed becomes completely accessible. In case of a lack of detection, the surviving posterior probability is completely

¹We have also investigated the LHC configuration with $\sqrt{s} = 7 \text{ GeV}$ and $\text{IL} = 1 \text{ fb}^{-1}$, which is very close to what has already been achieved [76, 77, 78], and consequently, we omit our results for this case.

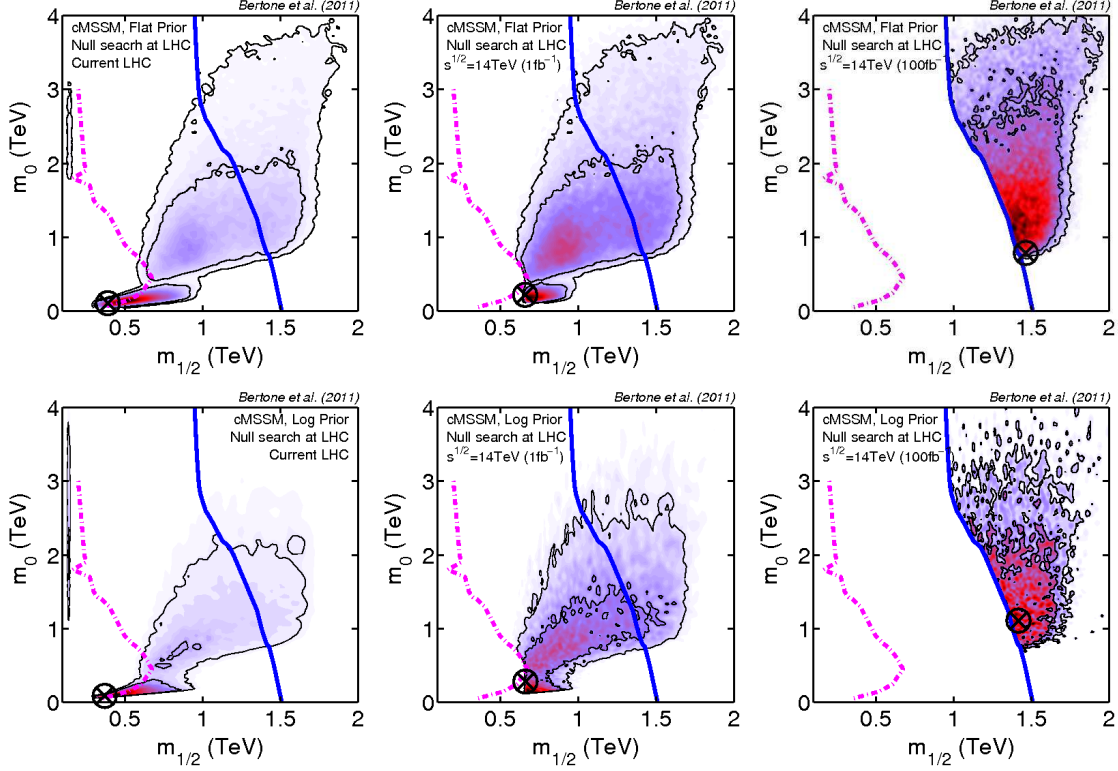


Figure 1: Posterior probability distribution for the cMSSM in the $(m_0, m_{1/2})$ plane, after null searches by the LHC with combinations of \sqrt{s} and integrated luminosities (IL) (left to right): Current LHC, 14 TeV and 1 fb^{-1} and 14 TeV and 100 fb^{-1} , for the priors (top) and log priors (bottom). The encircled black cross represents the best-fit point. The inner and outer solid, black contours delimit the 68% C.L. and 95% C.L. posterior regions respectively. We also illustrate the 5σ detection threshold of the LHC by the magenta dot-dashed curve for $\sqrt{s} = 14\text{ TeV}$ and $\text{IL} = 1\text{ fb}^{-1}$, and by the solid blue curve for $\sqrt{s} = 14\text{ TeV}$ and $\text{IL} = 100\text{ fb}^{-1}$.

confined to what, from here on, we call the funnel region, which encompasses the A -funnel and a small fraction of the focus point region which evades the current XENON-100 constraints, since it is pushed to large m_χ , for both choices of priors, as can be seen in the right-most panels of Fig. 1. The percentage of the currently favoured cMSSM parameter space which would survive a lack of detection at the LHC is given in Table 3, for both choices of priors. Those values can be interpreted as probabilities for the *nightmare* scenario in the cMSSM: for the LHC configuration with $\sqrt{s} = 14\text{ TeV}$ and $\text{IL} = 100\text{ fb}^{-1}$, the probability of a non-detection lies between about 3% and 36%, depending on the choice of priors, with the flat prior giving a larger probability to the nightmare scenario (as a larger fraction of its posterior probability lies in the funnel region, beyond the reach of the LHC).

3.2 Implications for Direct detection

In this section, we investigate the impact of hypothetical null searches at the LHC for

Prior	LHC Configuration (\sqrt{s} , IL)	
	14 TeV, 1 fb $^{-1}$	14 TeV, 100 fb $^{-1}$
Flat	93.8	36.0
Log	66.8	3.0

Table 3: Percentage of the currently favoured parameter space in the cMSSM that would survive a lack of SUSY detection at the LHC with the given configuration of centre of mass energy \sqrt{s} and integrated luminosity IL.

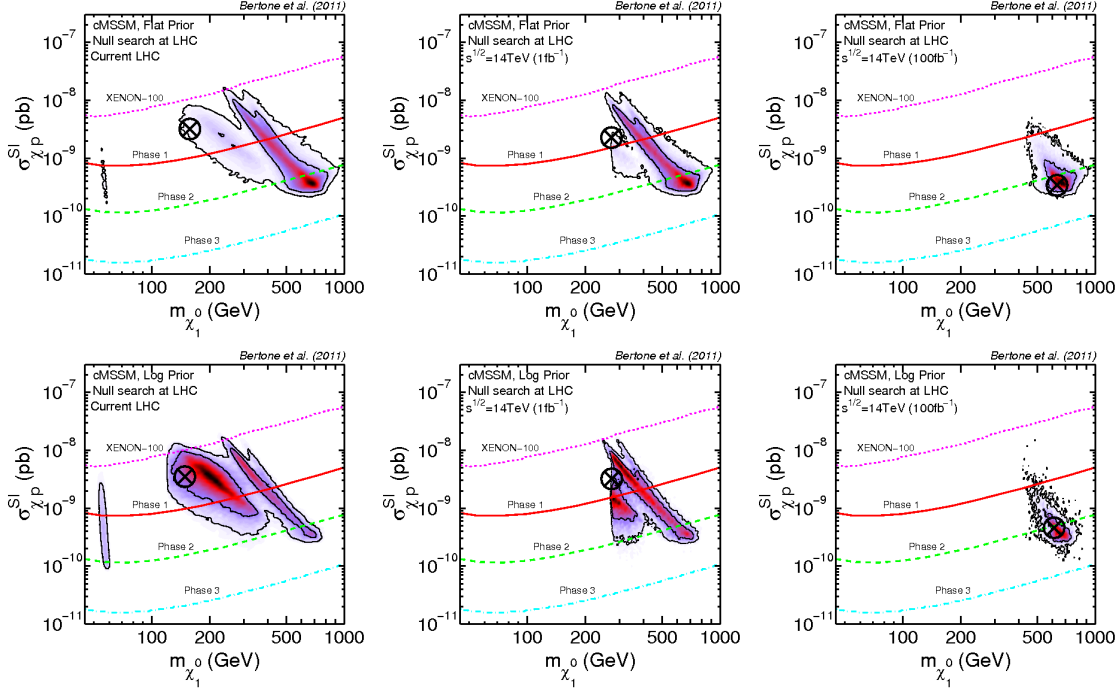


Figure 2: Favoured region in the cMSSM once current constraints and future null searches at the LHC are taken into account, for flat priors (top) and log priors (bottom). We assume null searches at the LHC with the following combinations of \sqrt{s} and integrated luminosities (from left to right): Current LHC, 14 TeV and 1 fb $^{-1}$, and 14 TeV and 100 fb $^{-1}$. The encircled black cross represents the best-fit point. The inner and outer solid, black contours delimit the 68% C.L. and 95% C.L. posterior regions respectively. We also show the current 90% C.L. exclusion limit from XENON-100 (magenta dotted), and the expected reach for for Phase 1 (solid red curve, expected to be reached by ~ 2012), Phase 2 (dashed green curve) and Phase 3 (dash-dotted cyan curve, expected to be reached around 2020) future direct detection experiments.

future ton-scale direct dark matter detectors.

In order to establish the prospects for *directly* detecting cMSSM DM, we need to make some assumptions regarding the local neutralino density and velocity distribution. A consistent way to combine accelerator and DD data is to impose the ‘scaling Ansatz’ discussed in [15], which rescales the local density of neutralinos according to their predicted cosmological relic density. Here, however, we focus on the regions of the cMSSM parameter space where the neutralino is the *sole* constituent of DM, by imposing a Gaussian likelihood

Experiment	Prior	LHC Configuration (\sqrt{s} , IL)		
		Current LHC	14 TeV, 1 fb $^{-1}$	14 TeV, 100 fb $^{-1}$
Direct detection, Phase 1	Flat	30.2	23.5	2.5
Direct detection, Phase 2		73.4	69.7	35.5
Direct detection, Phase 3		100.0	100.0	100.0
IceCube plus DeepCore		9.6	6.9	0.5
Direct detection, Phase 1	Log	68.6	35.7	1.2
Direct detection, Phase 2		95.8	89.0	31.1
Direct detection, Phase 3		100.0	100.0	100.0
IceCube plus DeepCore		16.8	11.1	0.2

Table 4: Fraction of the cMSSM parameter space surviving null searches at the LHC which can be probed by direct detection experiments or by IceCube (the latter after 5 years of observation). Those values represent the probability of discovery by the corresponding experiment (for each prior choice) assuming the LHC fails to discover SUSY at the given energy and integrated luminosity.

on $\Omega_\chi h^2$ (see Table I), and therefore the scaling Ansatz becomes almost irrelevant.

For an easier comparison with the existing literature we have fixed the astrophysical parameters describing the density and velocity distribution of DM particles to the commonly adopted benchmark values: local CDM density $\rho_{\odot, \text{CDM}} = 0.4 \text{ GeV cm}^{-3}$; circular velocity $v_0 = 235 \text{ km s}^{-1}$ and escape velocity $v_{esc} = 550 \text{ km s}^{-1}$ (see, e.g., [26] and references therein for a recent discussion of the astrophysical uncertainties relating to these quantities). We have also neglected hadronic uncertainties in WIMP-nucleon couplings, adopting for the light quarks contribution to the nucleon form factors the values $f_{Tu} = 0.02698$, $f_{Td} = 0.03906$ and $f_{Ts} = 0.36$ [82]. Accounting for such uncertainties by including them as nuisance parameters in the scan would only mildly change the numerical results presented here, but the main conclusions would remain unchanged, in agreement with the findings of [15, 14].

In Fig. 2, we display the results of the posterior probability distribution of the cMSSM in the $(m_\chi, \sigma_{\chi p}^{\text{SI}})$ plane following our scan corresponding to null searches at the LHC with the same priors and combinations of \sqrt{s} and integrated luminosities as displayed in Fig. 1. For comparison, the expected sensitivity of upcoming direct detection experiments is also shown for the following experimental setups:

- **Phase 1:** experiments will probe cross sections down to $\sigma_{\chi p}^{\text{SI}} \sim 10^{-9} \text{ pb}$, corresponding to the projected sensitivity of SuperCDMS at SNOLab [83] with a detector target mass of 27 kg operating for 1 year (solid red curve), roughly equivalent to the reach of XENON-100 by the end of 2012.
- **Phase 2:** experiments will probe cross sections down to $\sigma_{\chi p}^{\text{SI}} \sim 10^{-10} \text{ pb}$, corresponding to the projected sensitivity of SuperCDMS at SNOLab with a detector target mass of 145 kg running for 3 years (dashed green curve).
- **Phase 3:** experiments will probe cross sections down to $\sigma_{\chi p}^{\text{SI}} \sim 10^{-11} \text{ pb}$, correspond-

ing to the projected sensitivity of SuperCDMS at SNOLab with a detector target mass of 1500 kg running for 4 years (dashed green curve), that should become available by 2021 [83]. The Xenon1T is expected to reach a sensitivity of $\sigma_{\chi\text{p}}^{\text{SI}} = 4 \times 10^{-11}$ pb by 2015 [84], and therefore to go down to $\sigma_{\chi\text{p}}^{\text{SI}} \sim 10^{-11}$ pb on a similar timescale as SuperCDMS.

The left panels of Fig. 2 show the favoured cMSSM region with current LHC data, for flat (top) and log (bottom) priors. Table 4 summarizes the percentage of our points that reside outside of the reach of the LHC, i.e., in the nightmare scenario (for a given configuration) that are detectable for each of the experimental direct detection phases described above.

The h -pole, stau co-annihilation and funnel regions displayed in the corresponding plots of Fig. 1 can be observed in Fig. 2 as “islands” in the parameter space bound by 68% C.L. contours and spanning the approximate mass ranges: $50 \text{ GeV} \lesssim m_\chi \lesssim 60 \text{ GeV}$, $100 \text{ GeV} \lesssim m_\chi \lesssim 500 \text{ GeV}$ and $200 \text{ GeV} \lesssim m_\chi \lesssim 1 \text{ TeV}$ respectively, with the best-fit point from current data (left panels) being located in the stau co-annihilation region for both priors.

Large portions of these three regions are within reach of Phase 1 direct detection experiments, which will be able to detect between 30% and 68% (depending on the choice of priors) of the parameter space currently outside the reach of the LHC. For both choices of priors, we observe that Phase 2 experiments will cover a substantially larger fraction of the currently surviving parameter space, between 73% and 95% for flat and log priors, respectively. Phase 3 experiments are expected to cover entirely the most probable region of the cMSSM currently inaccessible to the LHC, a result that, as we shall see, holds true also for the ultimate reach of the LHC.

After its ~ 18 month shutdown period starting in 2013, the LHC will be brought up to $\sqrt{s} = 14 \text{ TeV}$. The central panel of Fig. 2 shows the implications for direct detection assuming $\text{IL} = 1 \text{ fb}^{-1}$. The LHC data in this case will rule out the h -pole region and start to cut in to the stau co-annihilation region, pushing the neutralino mass to larger values (see Fig. 4 below) and substantially reducing the percentage of surviving points within the reach of Phase 1 DD experiments, from 30% to 23% for flat priors, and from 68% to 35% for log priors. The prospects for detection with Phase 2 DD experiments remain fairly stable, while, again, Phase 3 DD experiments can probe all of the surviving parameter space.

Lastly, for $\sqrt{s} = 14 \text{ TeV}$ and $\text{IL} = 100 \text{ fb}^{-1}$, as expected from Fig. 1, for both flat and log prior scans the h -pole and stau co-annihilation regions are now fully accessible to the LHC, with the inaccessible part of the funnel region being quite similar for either set of priors. In both cases, we can see from Table 4 that, whilst a small percentage (of order 1 – 2%) of points are accessible to the Phase 1 experiments. It is clear that Phase 2 detectors will be necessary in order to have a significant chance (i.e., of order $\sim 30\%$, independently of the

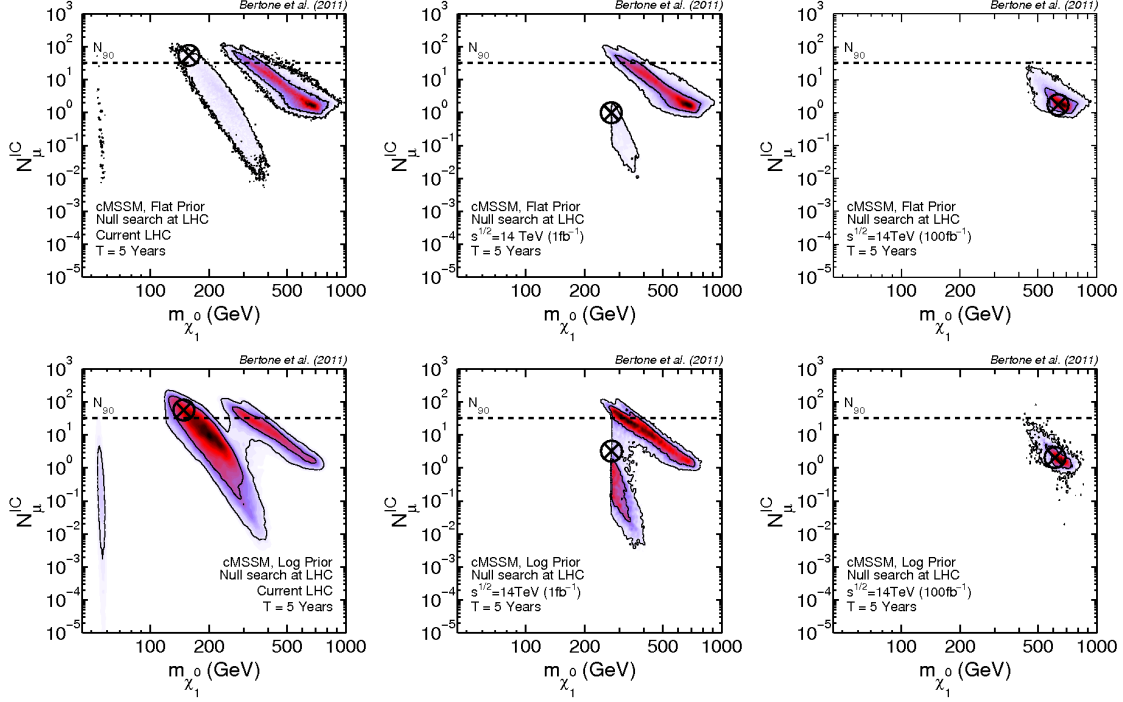


Figure 3: Posterior probability distribution of the cMSSM, displayed in the $(m_{\chi}, N_{\mu}^{\text{IC}})$ plane, corresponding to null searches by the LHC with combinations of \sqrt{s} and integrated luminosities (from left to right): Current LHC, 7 TeV and 1 fb^{-1} , 14 TeV and 1 fb^{-1} , and 14 TeV and 100 fb^{-1} , when using flat priors (top) and log priors (bottom). The number of muon events N_{μ}^{IC} assumes 5 years of observations by IceCube plus DeepCore. The encircled black cross represents the best-fit point. The inner and outer solid, black contours delimit the 68% C.L. and 95% C.L. posterior regions respectively. The horizontal dashed line gives the 90% C.L. detection threshold, and the encircled black cross is the best-fit in each scenario.

choice of priors) of discovering dark matter in the context of the cMSSM, whose gaugino and scalar mass parameters would in this case be located in the high mass funnel region, if it evades discovery by the LHC in the long term.

Interestingly, we find that even in the case of null searches at the LHC with $\sqrt{s} = 14 \text{ TeV}$ and $\text{IL} = 100 \text{ fb}^{-1}$, i.e., after many years of data taking after 2014, 100% of the cMSSM posterior will be probed by Phase 3 DD experiments, that will become available on a similar timescale.

3.3 Implications for indirect detection with the IceCube neutrino telescope

In this section we examine the prospects for detecting DM in the cMSSM with indirect searches in the nightmare scenario, focusing on the detection of high energy neutrinos from the Sun. Dark Matter particles are expected to scatter off nuclei in the Sun, and to sink at

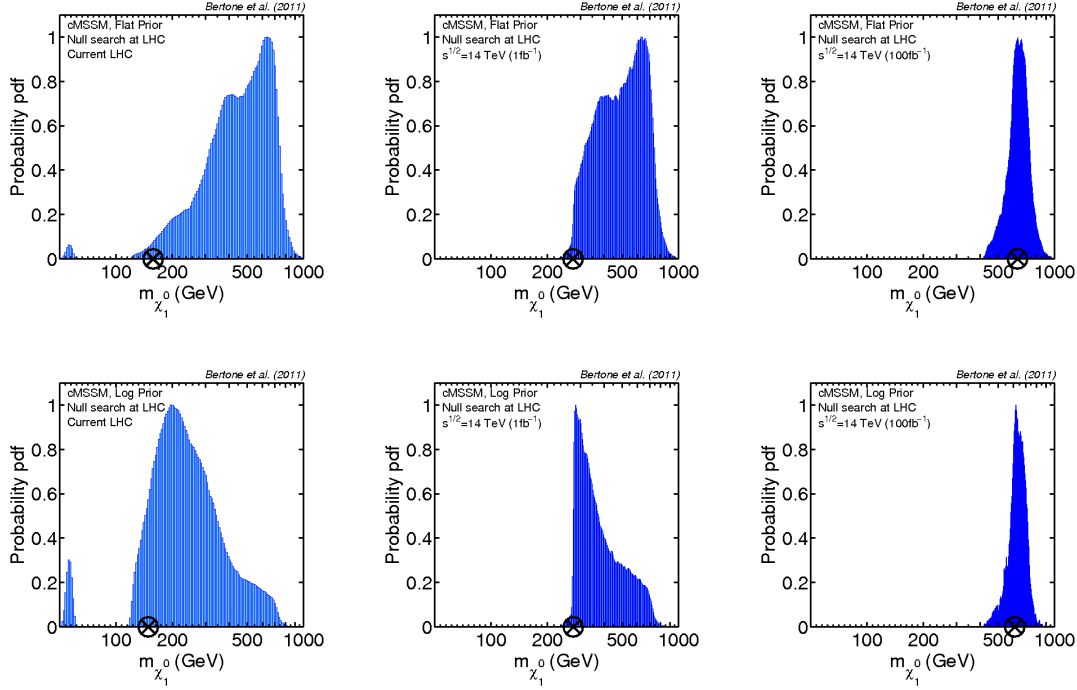


Figure 4: 1D pdf for the neutralino mass m_χ for flat priors (top) and log priors (bottom), assuming Current LHC constraints (left), null searches at the LHC with $\sqrt{s}=14$ TeV and $IL=1$ fb $^{-1}$ (middle) and null searches at the LHC with $\sqrt{s}=14$ TeV and $IL=100$ fb $^{-1}$ (right panels). The encircled black cross represents the best-fit point.

its centre, where they can subsequently annihilate. Among the annihilation products only neutrinos can escape, and produce a neutrino flux on Earth that is currently searched for with the IceCube neutrino telescope, located at the South Pole (see, e.g., [39]). IceCube is now fully built, with 80 strings in total, and it has been recently supplemented by a more densely instrumented region (consisting of six additional strings) at its core, called DeepCore (see, e.g., [86, 85]), which has the effect of lowering its neutrino energy threshold, E_ν^{th} , to approximately 10 GeV and increasing the effective area for low-energy events [87].

The number of neutrino-induced muon events, N_μ^{IC} , observable by IceCube from the direction of the Sun can be computed as

$$N_\mu^{\text{IC}} = \int_{\Delta\Omega_\odot} d\Omega \int_{E_\nu^{\text{th}}}^\infty A_\nu^{\text{eff}}(E_\nu) \frac{d\Phi_\nu}{dE_\nu} dE_\nu \quad (3.1)$$

where $\frac{d\Phi_\nu}{dE_\nu}$ is the incident muon neutrino flux at the detector, E_ν^{th} is the energy threshold, and $A_\nu^{\text{eff}}(E_\nu)$ is the muon neutrino effective area of the detector for muon neutrinos with energy E_ν , averaged over the northern hemisphere. The flux is then integrated over the solid angle $\Delta\Omega_\odot$ subtended by the Sun, corresponding to a cone with half-angle of approximately 0.3° .

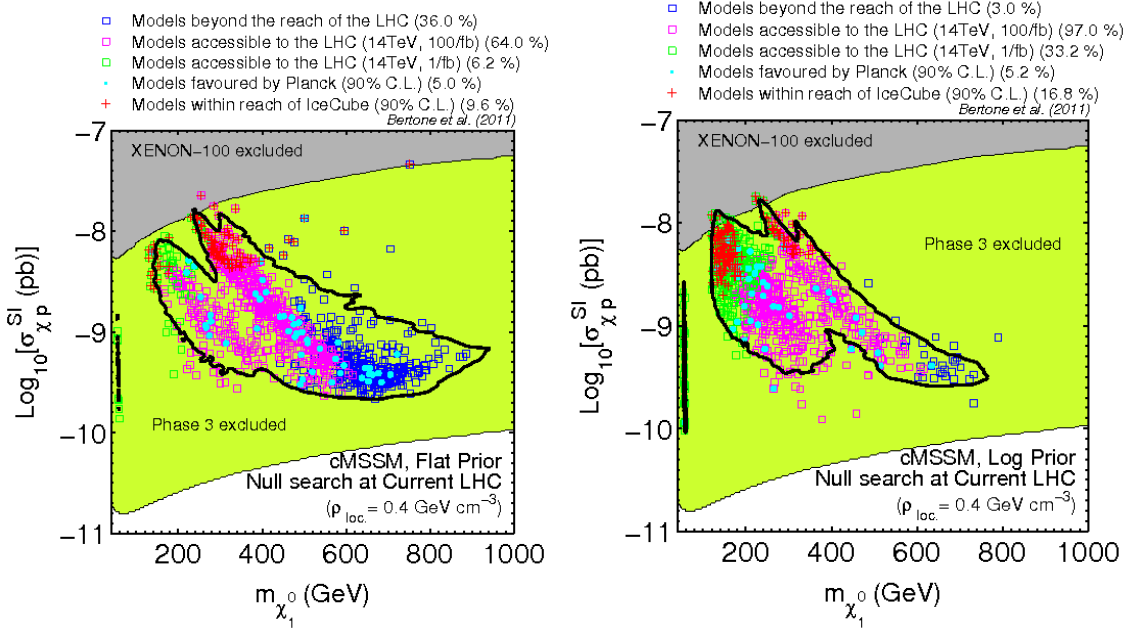


Figure 5: Summary of the reach of various probes in the m_{χ} vs $\sigma_{\chi\text{p}}^{\text{SI}}$ plane for flat priors (left) and log priors (right) for samples resulting from a null search using the current configuration of the LHC. The solid, black contour delimits the 95% posterior region from current data (including Current LHC constraints). Equal weight samples from the posterior are shown and are coloured (and thinned by a factor of two for display purposes) as follows: green (magenta) squares are accessible to the LHC with $\sqrt{s} = 14 \text{ TeV}$ and $\text{IL} = 1 \text{ fb}^{-1}$ ($\text{IL} = 100 \text{ fb}^{-1}$); blue squares are outside the reach of the LHC with $\sqrt{s} = 14 \text{ TeV}$ and $\text{IL} = 100 \text{ fb}^{-1}$ (nightmare scenario); cyan filled circles are expected to be favoured at 90% C.L. by Planck; red crosses are accessible to IceCube. The yellow shaded region represents the reach of future Phase 3 direct detection experiments.

The capture rate is computed using `DarkSUSY v5.05` assuming, as above, a local CDM density $\rho_{\odot} = 0.4 \text{ GeV cm}^{-3}$ and a Maxwell-Boltzmann velocity distribution with mean $\bar{v} = 235 \text{ km s}^{-1}$. In order to assess the prospects for discovering DM with IceCube, the expected signal, given by Eq. (3.1), must be compared with the the expected number of background events arising from the following sources:

- down-going muon events produced in a single cosmic ray shower in the southern hemisphere;
- muon events, misreconstructed as upgoing, resulting from two simultaneous cosmic ray showers in the southern hemisphere;
- an isotropic background of neutrino-induced muon events generated by atmospheric neutrinos;
- neutrino-induced muon events generated by cosmic neutrinos;

v) and muon events generated by neutrinos produced by cosmic-ray interactions in the solar corona.

We follow a methodology similar to that adopted in [88] and we only consider events from the direction of the Sun when it resides in the northern hemisphere, thereby eliminating contribution from (i). The contribution from (ii) can be reduced to negligible levels by using appropriate analysis cuts and therefore it is reasonable to assume that IceCube can reject such a background [89]. The isotropic background contribution from cosmic neutrinos (i.e., background (iv)) can be safely neglected (we estimate it to be approximately 5×10^{-3} events per year), as well as the background contribution (v) from cosmic-ray interactions in the solar corona, which we calculate to be approximately 5×10^{-4} events per year. Our estimate of background due to up-going atmospheric neutrinos (iii) is obtained by substituting into Eq. (3.1) the best-fit measurements for the isotropic atmospheric neutrino flux from SuperKamiokande and AMANDA II presented in Fig. 10 of [90], leading to an expected background, $\langle n_b \rangle$, of approximately 4.9 events per year. From this background, the number of muon events corresponding to a 90% C.L. detection threshold can be estimated using the Feldman-Cousins construction [91], giving $N_{90} = 32$ events for a 5 year period.

In Fig. 3 we display the posterior probability distribution of the cMSSM, in the $(m_\chi, N_\mu^{\text{IC}})$ plane, corresponding to null searches by the LHC with combinations of \sqrt{s} and integrated luminosities as in Figs. 1 and 2 for flat (upper) and log (lower) priors on cMSSM input parameters. We also display the corresponding number of events associated with the 90% C.L. Feldman-Cousins sensitivity estimate N_{90} (dashed line). In Table 4 we list the percentage of points inaccessible to the LHC that are detectable by IceCube (i.e., above the N_{90} threshold) for each of our investigated LHC configurations. The left panels of Fig. 3 correspond to the current LHC configuration. For our log prior we can clearly identify the h -pole, stau co-annihilation and funnel regions as the 68% C.L. regions spanning the mass ranges $50 \text{ GeV} \lesssim m_\chi \lesssim 60 \text{ GeV}$, $100 \text{ GeV} \lesssim m_\chi \lesssim 500 \text{ GeV}$ and $200 \text{ GeV} \lesssim m_\chi \lesssim 1 \text{ TeV}$ respectively. The distribution of probability in these regions is extremely similar to that displayed in Fig. 2 for the $(m_\chi, \sigma_{\chi\text{p}}^{\text{SI}})$ plane. Despite the fact that each of these three regions are partially accessible to IceCube, only up to $\sim 17\%$ of the samples currently outside the reach of the LHC can actually be probed. For flat priors, both the stau co-annihilation and funnel regions are partially accessible (the h -pole region is barely visible due to the resolution of the scan), but the relative suppression of the stau co-annihilation region with respect to the log priors leads to an even smaller percentage, $\sim 10\%$, of detectable samples.

The central panels of Fig. 3 correspond to $\sqrt{s} = 14 \text{ TeV}$ and $\text{IL} = 1 \text{ fb}^{-1}$. In analogy with the corresponding results in Fig. 2, the h -pole region and a large portion of the stau co-annihilation region are probed by the LHC, and therefore ruled out in case of null searches. This leads to a shift of the posterior to higher neutralino masses, and to an enhancement in correspondence of the funnel region, which tends to reside for linear priors

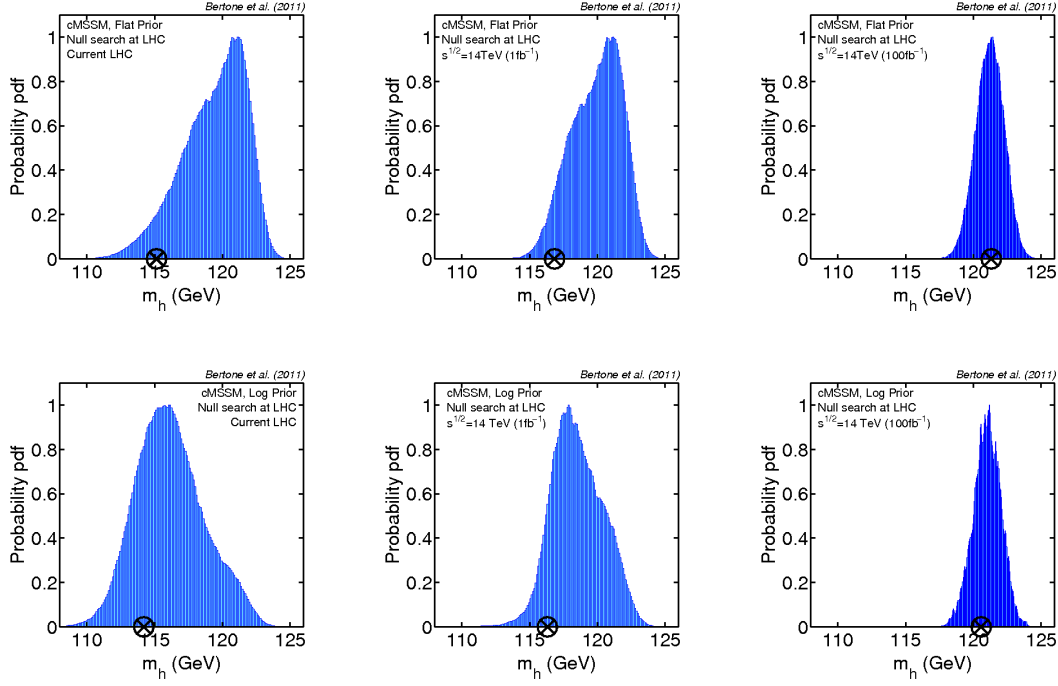


Figure 6: 1D pdf for the lightest Higgs mass m_h for flat priors (top) and log priors (bottom), assuming Current LHC constraints (left), null searches at the LHC with $\sqrt{s}=14$ TeV and $\text{IL}=1\text{ fb}^{-1}$ (middle) and null searches at the LHC with $\sqrt{s}=14$ TeV and $\text{IL}=100\text{ fb}^{-1}$ (right panels). The encircled black cross represents the best-fit point.

at $m_\chi \sim 500\text{ GeV}$ and $N_\mu^{\text{IC}} \lesssim 10$, hence inaccessible to IceCube. For log priors, the neutralino mass is shifted towards lower values, and N_μ^{IC} towards slightly higher values, leading to a larger probability of detection, 11%, to be compared with 6.9% in the case of flat priors.

Finally, for $\sqrt{s}=14\text{ TeV}$ and $\text{IL}=100\text{ fb}^{-1}$ (right panels), IceCube will have little impact in probing the cMSSM in case of null searches at the LHC, for either sets of priors, resulting in detection probabilities in the range $0.1 - 1\%$.

We have also verified that for all LHC configurations, the entire parameter space fraction accessible to IceCube will also be accessible to Phase 1 direct detection experiments (but not vice-versa). This means that IceCube on its own is not expected to be able to improve constraints with respect to even Phase 1 direct detectors. However, it will provide a valuable independent cross check in at least a subset of the parameter space. This is obviously important in terms of evaluating and reducing systematic effects, e.g., from astrophysical uncertainties, that would affect both direct and indirect detection limits.

Several features in Figs. 2 and 3 can be better understood upon inspection of the 1D pdf for m_χ , shown in Fig. 4 for the same LHC configurations and same priors. The h -pole, stau co-annihilation and funnel regions can be roughly identified in the left panels, and

the progressive shift towards large m_χ as the LHC cuts into the stau co-annihilation and funnel regions is apparent from the central and right panels. It is also clear from this figure that the prior dependency of the results decreases as more and more constraining data are accumulated (left to right), as expected.

Our results are summarized in Fig. 5, which shows in a more concise way the parameter space accessible to various observational channels in the $(m_\chi, \sigma_{\chi p}^{\text{SI}})$ plane, for both choices of priors. For this figure, we have additionally investigated which fraction of the parameter space that can be potentially ruled out by a more accurate determination of the relic abundance by the Planck satellite, which is expected to tighten current cosmological limits on the DM relic density by a factor of ~ 10 (see, e.g., [92]). We find that about 95% of the cMSSM parameter space outside the reach of the LHC will be potentially ruled out by Planck (at the 90% C.L.), independently of the assumed LHC configuration. This is because models with the “correct” relic density (i.e., matching the current determination by WMAP within Planck sensitivity) are essentially uniformly spread throughout the $(m_0, m_{1/2})$ plane (see the cyan samples in Fig. 5). Therefore, Planck has almost uniform power in probing them, independently of the parameter space fraction excluded by the LHC. Fig. 5 also clarifies that the reach of IceCube lies just below the current direct detection exclusion limits from XENON-100 (red crosses), while the LHC nightmare scenario (i.e., the region inaccessible to the LHC with $\sqrt{s} = 14 \text{ TeV}$ and $\text{IL} = 100 \text{ fb}^{-1}$, indicated here by the blue squares) is confined to higher neutralino mass regions of the parameter space, corresponding to spin-independent cross sections in the range $\sigma_{\chi p}^{\text{SI}} \sim 10^{-9} - 10^{-10} \text{ pb}$. It is again apparent that Phase 3 DD experiments will be able to probe the entire surviving cMSSM parameter space, including the nightmare region. As mentioned above, further inclusion of astrophysical and hadronic uncertainties in the analysis is unlikely to change this conclusion, as the reach of Phase 3 DD experiments lies comfortably below the favoured parameter space.

3.4 The role of the Higgs

What is the role of the Higgs boson in this scenario? Obviously, a detection of the Higgs in the next few years would provide crucial information, but since we do not know if, and at which mass, it will be detected, we can only discuss what consequences the possible outcomes of Higgs searches would have on our scenario.

To this aim, we have calculated the 1D pdf for the lightest Higgs mass m_h , shown in Fig. 6 for the same LHC configurations and same priors as in Figs. 2 and 3. In the so-called decoupling limit, the lightest Higgs couplings to Standard Model particles are identical to those of the Standard Model Higgs [93]. This happens when $m_A \gg m_Z$, a condition that is fulfilled for large values of $m_{1/2}$. Upon inspection of Fig. 1, we see that the posterior is indeed pushed towards large values of $m_{1/2}$, especially in the right-most plots, corresponding to $\text{IL} = 100 \text{ fb}^{-1}$ of data at $\sqrt{s} = 14 \text{ TeV}$.

A recent analysis of the prospects for detecting the Standard Model Higgs boson at ATLAS [94], has shown that $\text{IL} = 2 \text{ fb}^{-1}$ of data at $\sqrt{s} = 8 \text{ TeV}$ will be sufficient to exclude

Standard Model Higgs masses between 114 and 500 GeV at the 95% CL. Since our 1D pdf's for null searches at the LHC with 14 TeV fall in the range 115–125 GeV, we can conclude that if the LHC will be able to rule out the Higgs in this range, then the cMSSM will be excluded. On the other hand, a 5σ discovery of the Higgs might take a much larger luminosity and might require running at larger energies. So if by the end of 2012 the LHC will have failed to rule out the last remaining window for the Higgs (currently, between 115 and 140 GeV, considering the recently presented results from the ATLAS and CMS combination of $1.6 + 1.6 \text{ fb}^{-1}$ of data [95]), then the future generation of direct detection experiment will have a good chance of discovering dark matter (within the cMSSM framework considered here).

4. Discussion and Conclusions

In this study we have quantitatively assessed the potential for discovering the cMSSM in case of null searches at the LHC (the “nightmare scenario” of particle physics), with future direct detection experiments and with the IceCube neutrino telescope.

Our main conclusion is that Phase 3 direct detection experiments (that can reach cross sections down to $\sigma_{\text{XP}}^{\text{SI}} \sim 10^{-11} \text{ pb}$) will be able to probe entirely the favoured region of the cMSSM parameter space in the nightmare scenario of particle physics, therefore providing a unique opportunity to test SUSY even in case of null searches at the LHC. Interestingly, these experiments are expected to be built on a timescale of 5–10 years, similar to that required for the LHC to reach $\text{IL} = 100 \text{ fb}^{-1}$ of data at $\sqrt{s} = 14 \text{ TeV}$.

In our analysis, we fixed all astrophysical parameters to the standard values commonly adopted in the literature. In principle, however, one should take into account all particle physics and astrophysical uncertainties in order to combine in a self-consistent fashion accelerator and particle astrophysics experiments [15, 26, 96]. Including the uncertainty on the local DM density [97, 98] would not change the fraction of cMSSM points accessible to direct detection experiments, since the SUSY points and the sensitivity curves would be rescaled by the same quantity (i.e., the ratio of the ‘true’ local density over the value adopted here). A more careful treatment of the velocity distribution and of the hadronic uncertainties in the neutralino-nucleon cross-section may instead have a stronger impact on direct and indirect searches [82, 99, 96], but given the ample margin between the bulk of the nightmare cMSSM parameter space and the sensitivity of Phase 3 direct detection experiments, it is unlikely that our main conclusion would change significantly.

Finally we have studied the implications of Higgs searches at the LHC, and we have shown that if a Standard Model-like Higgs is not found at the LHC with $\text{IL} = 100 \text{ fb}^{-1}$ of data at $\sqrt{s} = 14 \text{ TeV}$, that would basically rule out the cMSSM, while an actual detection in the appropriate mass range would provide additional motivation to continue the study of Supersymmetry with astroparticle experiments.

Acknowledgments

We would like to thank Carlos Perez de los Heros for his advice regarding IceCube and DeepCore and our co-authors of Ref. [14] for providing us with the MultiNest samples obtained in their work. DTC is supported by the Science and Technology Facilities Council. Part of this work was conducted while DTC was at CERCA Case Western Reserve University, supported by NASA grant 4200188792 and also supported in part by the US DoE. R. RdA would like to thank the support of the Spanish MICINN's Consolider-Ingenio 2010 Programme under the grant MULTIDARK CSD2209-00064. R.T. would like to thank the Kavli Institute for Theoretical Physics, Santa Barbara, for hospitality. This research was supported in part by the National Science Foundation under Grant No. PHY05-51164.

References

- [1] G. Bertone, (ed.), Cambridge, UK: Univ. Pr. (2010) 738 p.
- [2] S. Chatrchyan *et al.* [CMS Collaboration], [arXiv:1103.0953 [hep-ex]].
- [3] V. Khachatryan *et al.* [CMS Collaboration], Phys. Lett. **B698** (2011) 196-218. [arXiv:1101.1628 [hep-ex]].
- [4] G. Aad *et al.* [Atlas Collaboration], [arXiv:1102.5290 [hep-ex]].
- [5] G. Aad *et al.* [Atlas Collaboration], arXiv:1102.2357 [hep-ex].
- [6] G. Aad *et al.* [ATLAS Collaboration], arXiv:1103.4344 [hep-ex].
- [7] G. Aad *et al.* [ATLAS Collaboration], arXiv:1103.6214 [hep-ex].
- [8] O. Buchmueller, R. Cavanaugh, D. Colling, A. De Roeck, M. J. Dolan, J. R. Ellis, H. Flacher, S. Heinemeyer *et al.*, [arXiv:1102.4585 [hep-ph]].
- [9] B. C. Allanach, [arXiv:1102.3149 [hep-ph]].
- [10] S. Akula, D. Feldman, Z. Liu, P. Nath, G. Peim, [arXiv:1103.5061 [hep-ph]].
- [11] M. Farina, M. Kadastik, D. Pappadopulo, J. Pata, M. Raidal and A. Strumia, Nucl. Phys. B **853** (2011) 607 [arXiv:1104.3572 [hep-ph]].
- [12] A. Strumia, [arXiv:1101.2195 [hep-ph]].
- [13] O. Buchmueller *et al.*, arXiv:1106.2529 [hep-ph].
- [14] G. Bertone, D. G. Cerdeno, M. Fornasa, R. R. de Austri, C. Strece and R. Trotta, arXiv:1107.1715 [hep-ph].
- [15] G. Bertone, D. G. Cerdeno, M. Fornasa, R. R. de Austri and R. Trotta, Phys. Rev. D **82** (2010) 055008 [arXiv:1005.4280 [hep-ph]].
- [16] G. Bertone, Nature **468** (2010) 389-393. [arXiv:1011.3532 [astro-ph.CO]].
- [17] R. L. Arnowitt and P. Nath, Phys. Rev. Lett. **69** (1992) 725.
- [18] G. G. Ross and R. G. Roberts, Nucl. Phys. B **377** (1992) 571.
- [19] V. D. Barger, M. S. Berger and P. Ohmann, Phys. Rev. D **49** (1994) 4908 [hep-ph/9311269].

- [20] G. L. Kane, C. F. Kolda, L. Roszkowski and J. D. Wells, *Phys. Rev. D* **49** (1994) 6173.
- [21] See, e.g., H. P. Nilles, *Phys. Rept.* **110** (1984) 1;
A. Brignole, L. E. Ibañez and C. Muñoz, *Perspectives on Supersymmetry*, ed. G. L. Kane, 125.
- [22] L. Bergstrom, *Rept. Prog. Phys.* **63**, 793 (2000) [arXiv:hep-ph/0002126].
- [23] C. Munoz, *Int. J. Mod. Phys. A* **19**, 3093 (2004) [arXiv:hep-ph/0309346].
- [24] G. Bertone, D. Hooper and J. Silk, *Phys. Rept.* **405** (2005) 279 [arXiv:hep-ph/0404175].
- [25] J. L. Feng, *Ann. Rev. Astron. Astrophys.* **48**, 495 (2010). [arXiv:1003.0904 [astro-ph.CO]].
- [26] M. Pato, L. Baudis, G. Bertone, R. Ruiz de Austri, L. E. Strigari, R. Trotta, *Phys. Rev. D* **83** (2011) 083505. [arXiv:1012.3458 [astro-ph.CO]].
- [27] R. Bernabei *et al.*, *Eur. Phys. J. C* **67** (2010) 39 [arXiv:1002.1028 [astro-ph.GA]].
- [28] C. E. Aalseth *et al.* [CoGeNT collaboration], arXiv:1002.4703 [astro-ph.CO].
- [29] C. E. Aalseth, P. S. Barbeau, J. Colaresi, J. I. Collar, J. D. Leon, J. E. Fast, N. Fields, T. W. Hossbach *et al.*, [arXiv:1106.0650 [astro-ph.CO]].
- [30] D. Hooper, J. I. Collar, J. Hall, D. McKinsey, *Phys. Rev. D* **82**, 123509 (2010). [arXiv:1007.1005 [hep-ph]].
- [31] E. Aprile *et al.* [XENON100 Collaboration], *Phys. Rev. Lett.* **105**, 131302 (2010) [arXiv:1005.0380 [astro-ph.CO]].
- [32] Z. Ahmed *et al.* [CDMS-II Collaboration], arXiv:1011.2482 [astro-ph.CO].
- [33] C. Savage, G. Gelmini, P. Gondolo and K. Freese, arXiv:1006.0972 [astro-ph.CO].
- [34] F. Bezrukov, F. Kahlhoefer and M. Lindner, arXiv:1011.3990 [astro-ph.IM].
- [35] C. Arina, J. Hamann, Y. Y. Y. Wong, [arXiv:1105.5121 [hep-ph]].
- [36] T. Schwetz, J. Zupan, [arXiv:1106.6241 [hep-ph]].
- [37] Adriani O. *et al.* [PAMELA Collaboration], *Nature* **458** 607-609 [arXiv:0810.4995 [astro-ph]] (2009)
- [38] Silk J., Olive K.A. and Srednicki M., *Phys. Rev. Lett.* **55** 257-259 (1985)
- [39] Halzen F. and Hooper D., *New J. Phys.* **11** 105019 [arXiv:0910.4513 [astro-ph.HE]]. (2009)
- [40] G. Jungman, M. Kamionkowski and K. Griest, *Phys. Rept.* **267**, 195 (1996) [arXiv:hep-ph/9506380].
- [41] R. Kitano, H. Ooguri and Y. Ookouchi, arXiv:1001.4535 [hep-th].
- [42] R. Trotta, R. R. de Austri and C. P. d. Heros, *JCAP* **0908** (2009) 034.
- [43] F. Feroz, B. C. Allanach, M. Hobson, S. S. AbdusSalam, R. Trotta and A. M. Weber, *JHEP* **0810**, 064 (2008) [arXiv:0807.4512 [hep-ph]].
- [44] R. Trotta, *Contemporary Physics*, **49**, 2, (2008) 71-104.
- [45] F. Feroz and M. P. Hobson, *Mon. Not. Roy. Astron. Soc.* **384** (2008) 449.
F. Feroz, M. P. Hobson and M. Bridges, arXiv:0809.3437.
- [46] F. Feroz, M. P. Hobson and R. Trotta, arXiv:1001.0719 [astro-ph.IM].

- [47] Y. Akrami, P. Scott, J. Edsjo, J. Conrad and L. Bergstrom, JHEP **1004** (2010) 057 [arXiv:0910.3950 [hep-ph]].
- [48] R. Trotta, F. Feroz, M. P. Hobson, L. Roszkowski and R. Ruiz de Austri, JHEP **0812**, 024 (2008).
- [49] L. Roszkowski, R. Ruiz de Austri and R. Trotta, Phys. Rev. D **82**, 055003 (2010) [arXiv:0907.0594 [hep-ph]].
- [50] <http://lepewwg.web.cern.ch/LEPEWWG>.
- [51] In Proceedings of "TAU 2010 - The 11th International Workshop on Tau Lepton Physics", Manchester, UK, 13 - 17 September 2010. M. Davier *et al.*, arXiv:0906.5443 [hep-ph].
- [52] Heavy Flavor Averaging D. Asner *et al.*, arXiv:1010.1589
- [53] The CDF Collaboration, *Phys. Rev. Lett.* **97** (2006) 062003; *Phys. Rev. Lett.* **97** (2006) 242003.
- [54] B. Aubert *et al.* [BABAR Collaboration], arXiv:0808.1915 [hep-ex].
- [55] B. Aubert *et al.* [BABAR Collaboration], Phys. Rev. Lett. **100** (2008) 021801 [arXiv:0709.1698 [hep-ex]].
- [56] M. Antonelli *et al.* [FlaviaNet Working Group on Kaon Decays], arXiv:0801.1817 [hep-ph].
- [57] N. Jarosik *et al.*, arXiv:1001.4744 [astro-ph.CO].
- [58] The CDF Collaboration, *Search for $B_s \rightarrow \mu^+ \mu^-$ and $B_d \rightarrow \mu^+ \mu^-$ decays in $p\bar{p}$ collisions with CDF-II*, CDF note 8956 (August 2007).
- [59] The LEP Higgs Working Group, <http://lephiggs.web.cern.ch/LEPHIGGS>; G. Abbiendi *et al.* [the ALEPH Collaboration, the DELPHI Collaboration, the L3 Collaboration and the OPAL Collaboration, The LEP Working Group for Higgs Boson Searches], Phys. Lett. B **565**, 61 (2003).
- [60] W.-M. Yao *et al.*, *The Review of Particle Physics*, *J. Phys.* **G33** (2006) 1 and 2007 partial update for the 2008 edition.
- [61] R. R. de Austri, R. Trotta and L. Roszkowski, JHEP **0605**, 002 (2006) [arXiv:hep-ph/0602028].
- [62] By the CDF Collaboration and D0 Collaboration, arXiv:0803.1683 [hep-ex].
- [63] K. Hagiwara, A. D. Martin, D. Nomura and T. Teubner, Phys. Lett. B **649**, 173 (2007).
- [64] G. Degrossi, G. F. Giudice, Phys. Rev. **D58** (1998) 053007. [arXiv:hep-ph/9803384 [hep-ph]].
- [65] L. Roszkowski, R. Ruiz de Austri and R. Trotta, JHEP **0707** (2007) 075;
- [66] G. Degrossi, P. Gambino and P. Slavich, Comput. Phys. Commun. **179** (2008) 759 [arXiv:0712.3265 [hep-ph]].
- [67] G. Degrossi, P. Gambino and P. Slavich, Phys. Lett. B **635** (2006) 335 [arXiv:hep-ph/0601135].
- [68] G. D'Ambrosio, G. F. Giudice, G. Isidori and A. Strumia, Nucl. Phys. B **645**, 155 (2002) [arXiv:hep-ph/0207036].
- [69] J. Foster, K. Okumura and L. Roszkowski, Phys. Lett. B **609**, 102 (2005) [hep-ph/0410323].

- [70] F. Mahmoudi, Comput. Phys. Commun. **180**, 1579 (2009) [arXiv:0808.3144 [hep-ph]].
- [71] E. A. Baltz, M. Battaglia, M. E. Peskin and T. Wizansky, Phys. Rev. D **74** (2006) 103521.
- [72] G. Bertone, D. G. Cerdeno, M. Fornasa, L. Pieri, R. R. de Austri and R. Trotta, arXiv:1111.2607 [astro-ph.HE].
- [73] M. J. White and F. Feroz, JHEP **1007** (2010) 064 [arXiv:1002.1922 [hep-ph]].
- [74] The ATLAS collaboration, ATLAS-CONF-2010-035, 2010.
- [75] The ATLAS collaboration, ATL-PHYS-PUB-2010-010, 2010.
- [76] G. Aad *et al.* [ATLAS Collaboration], arXiv:1109.6572 [hep-ex].
- [77] ATLAS Collaboration, <https://atlas.web.cern.ch/Atlas/GROUPS/PHYSICS/CONFNOTES/ATLAS-CONF-2011-132/ATLAS-CONF-2011-132.pdf>.
- [78] S. Chatrchyan *et al.* [CMS Collaboration], arXiv:1109.2352 [hep-ex].
- [79] H. Baer, C. h. Chen, M. Drees, F. Paige and X. Tata, Phys. Rev. Lett. **79**, 986 (1997) [Erratum-ibid. **80**, 642 (1998)] [arXiv:hep-ph/9704457].
- [80] H. Baer, V. Barger, A. Lessa and X. Tata, JHEP **0909** (2009) 063 [arXiv:0907.1922 [hep-ph]].
- [81] H. Baer, C. h. Chen, M. Drees, F. Paige and X. Tata, Phys. Rev. D **59**, 055014 (1999) [arXiv:hep-ph/9809223].
- [82] J. R. Ellis, K. A. Olive and C. Savage, Phys. Rev. D **77** (2008) 065026 [arXiv:0801.3656 [hep-ph]].
- [83] http://www.fnal.gov/directorate/OPMO/Projects/SuperCDMS/WGM/2010/08_18/bauer_supercdms.pdf
- [84] http://xenon.astro.columbia.edu/talks/aprile_ucla_dm2010.pdf
- [85] C. Wiebusch and f. t. I. Collaboration, arXiv:0907.2263 [astro-ph.IM].
- [86] J. Ahrens *et al.* [IceCube Collaboration], Astropart. Phys. **20** (2004) 507 [arXiv:astro-ph/0305196].
- [87] D. Cowen for the IceCube Collaboration, *Proceedings of the 13th International Workshop On Neutrino Telescopes, 10-13 March 2009, Venice, Italy, pp. 253-262*
- [88] I. F. M. Albuquerque and C. Perez de los Heros, Phys. Rev. D **81** (2010) 063510 [arXiv:1001.1381 [astro-ph.HE]].
- [89] C. Perez de los Heros, *private communication (2010)*.
- [90] R. Abbasi *et al.* [IceCube Collaboration], Phys. Rev. D **79** (2009) 102005 [arXiv:0902.0675 [astro-ph.HE]].
- [91] G. J. Feldman and R. D. Cousins, Phys. Rev. D **57** (1998) 3873
- [92] http://www.rssd.esa.int/index.php?project=PLANCK&page=perf_top
- [93] A. Djouadi, Phys. Rept. **459** (2008) 1 [arXiv:hep-ph/0503173].
- [94] I. T. f. Collaboration, arXiv:1012.0694 [hep-ex].

- [95] Gigi Rolandi, *HPC*, November 2011,
<http://indico.in2p3.fr/getFile.py/access?contribId=72&sessionId=19&resId=0&materialId=slides&confId=6004>
- [96] P. D. Serpico, G. Bertone, Phys. Rev. **D82** (2010) 063505. [arXiv:1006.3268 [astro-ph.HE]].
- [97] M. Pato, O. Agertz, G. Bertone, B. Moore and R. Teyssier, Phys. Rev. D **82** (2010) 023531 [arXiv:1006.1322 [astro-ph.HE]].
- [98] P. Salucci, F. Nesti, G. Gentile and C. F. Martins, Astron. Astrophys. **523** (2010) A83 [arXiv:1003.3101 [astro-ph.GA]].
- [99] L. E. Strigari, R. Trotta, JCAP **0911** (2009) 019. [arXiv:0906.5361 [astro-ph.HE]].